NANO LETTERS
Letter
Cite This: Nano Lett. 2018, 18, 1849−1855
pubs.acs.org/NanoLett

Quantum-Confined Electronic States Arising from the Moiré Pattern of MoS_2−WSe_2 Heterobilayers

Yi Pan,[†,‡] Stefan Fölsch,[†] Yifan Nie,[§] Dacen Waters,[∥] Yu-Chuan Lin,[⊥] Bhakti Jariwala,[⊥] Kehao Zhang,[⊥] Kyeongjae Cho,[§] Joshua A. Robinson,[⊥] and Randall M. Feenstra*[,∥]

[†]Paul-Drude-Institut für Festkörperelektronik, Hausvogteiplatz 5-7, 10117 Berlin, Germany

[‡]Center for Spintronics and Quantum Systems, State Key Laboratory for Mechanical Behavior of Materials, Xi'an Jiaotong University, Xi'an 710049, China

[§]Dept. Materials Science and Engineering, The University of Texas at Dallas, Dallas, Texas 75080 United States

[∥]Dept. Physics, Carnegie Mellon University, Pittsburgh, Pennsylvania 15213 United States

[⊥]Dept. Materials Science and Engineering, and Center for 2-Dimensional and Layered Materials, The Pennsylvania State University, University Park, Pennsylvania 16802 United States

Supporting Information

ABSTRACT: A two-dimensional (2D) heterobilayer system consisting of MoS_2 on WSe_2, deposited on epitaxial graphene, is studied by scanning tunneling microscopy and spectroscopy at temperatures of 5 and 80 K. A moiré pattern is observed, arising from lattice mismatch of 3.7% between the MoS_2 and WSe_2. Significant energy shifts are observed in tunneling spectra observed at the maxima of the moiré corrugation, as compared with spectra obtained at corrugation minima, consistent with prior work. Furthermore, at the minima of the moiré corrugation, sharp peaks in the spectra at energies near the band edges are observed for spectra acquired at 5 K. The peaks correspond to discrete states that are confined within the moiré unit cells. Conductance mapping is employed to reveal the detailed structure of the wave functions of the states. For measurements at 80 K, the sharp peaks in the spectra are absent, and conductance maps of the band edges reveal little structure.

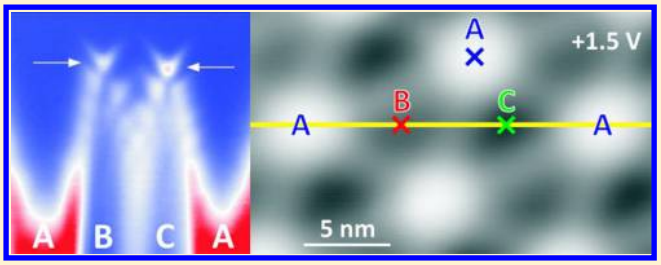

KEYWORDS: *2D materials, heterostructures, transition metal dichalcogenides, scanning tunneling microscopy, scanning tunneling spectroscopy*

Vertical heterostructures of various two-dimensional (2D) materials have been studied intensely over the past decade due to their novel electronic and optical properties.[1−4] Just as different electronic properties are found between 1 monolayer (ML) and 2 ML of a given material (e.g., MoS_2)[2,5] due to the hybridization of the electronic states between the layers, so too can a combination of two different materials (such as MoS_2 on WSe_2) be expected to produce electronic states that are not a simple combination of the states of the constituent materials.[6−12] Understanding in detail the hybridization effects that occur between specific 2D layers constitutes a very important topic, such that we might obtain some general understanding (and predictive capability) for arbitrary 2D layers that are combined together into a heterostructure.[13−15]

When two MLs of different 2D materials are combined to form a heterobilayer (or when rotational misalignment occurs between the lattice of MLs of the same 2D material), a moiré pattern will form.[16] Such patterns have been studied in detail, e.g., for graphene on h-BN,[17−20] and also for various transition-metal dichalcogenide (TMD) materials.[7,18,21,22] In a recent report, Zhang et al. described scanning tunneling microscopy and spectroscopy (STM−STS) obtained for heterobilayers of MoS_2 and WSe_2, with the measurements performed at a temperature near 77 K.[7] A moiré corrugation with relatively large amplitude of 0.17 nm (sample bias of +3 V) and a period of 8.7 ± 0.2 nm was observed. Significantly, shifts in the band-edge locations as large as 0.2 eV were found between tunneling spectra obtained at the maxima of this corrugation compared with spectra obtained from the two different kinds of minima. It was argued that hybridization of WSe_2-derived valence band (VB) states at the Γ-point in **k**-space, with resulting energy being quite sensitive to the MoS_2−WSe_2 separation, was a large contributor to the observed variation in the band-edge energies.

In our work, we also study vertical heterobilayers of MoS_2 on WSe_2, grown in our case by a combination of powder-vaporization chemical vapor deposition (CVD for MoS_2) and metal−organic chemical vapor deposition (MOCVD, for WSe_2).[8,23−25] STM−STS measurements were performed in a low-temperature STM system operated at a base temperature of 5 K. We employ a variable-z measurement method for the

Received: December 5, 2017
Revised: January 31, 2018
Published: February 7, 2018

DOI: 10.1021/acs.nanolett.7b05125
Nano Lett. 2018, 18, 1849−1855

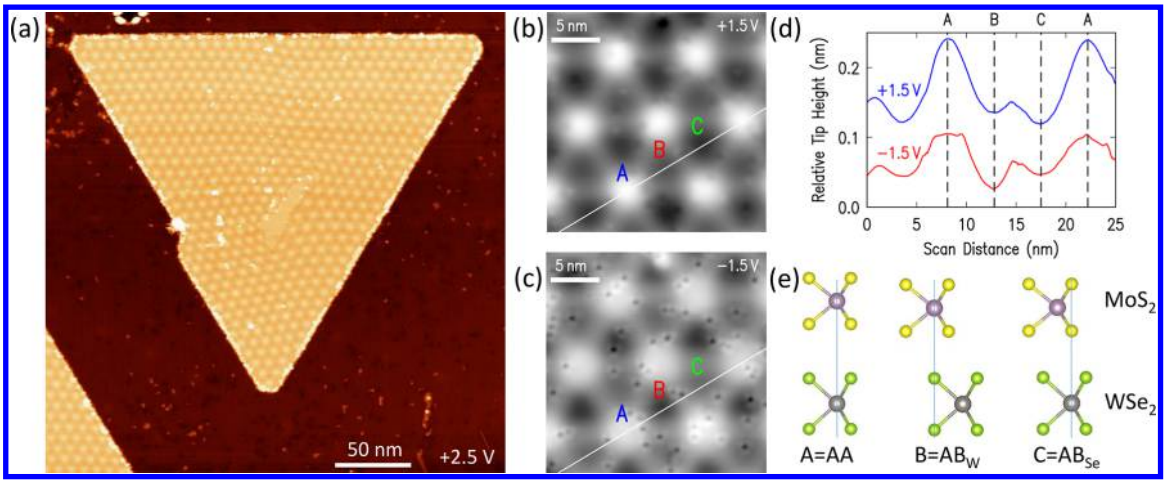

Figure 1. STM data acquired at 5 K, showing (a) a large-area image, (b, c) images acquired at +1.5 and −1.5 V, (d) cross-sectional cuts of inset images, and (e) a schematic view of respective registrations between MoS_2 and WSe_2; cases labeled A, B, and C correspond, using structural analysis and notation from ref 7, to AA, AB_W, and AB_{Se}.

STS, which ensures high dynamic range in the conductance (see the Supporting Information for details).[26] The STM−STS results that we obtain are very similar in many respects to those of Zhang et al.[7] In particular, we find a moiré corrugation with amplitude of 0.13 nm (sample bias of +1.5 V) and a period of 8.5 ± 0.2 nm, and spectral shifts as large as 0.2 eV are observed between tunneling spectra obtained at maxima of the corrugation compared with those obtained at the two inequivalent types of minima.

Additionally, for measurements performed at 5 K, we also observe narrow (<10 meV), sharp peaks that occur near band-edge energies of the spectra for both the valence band (VB) and the conduction band (CB). We argue that such states arise from quantum confinement in the spatially varying potential associated with the moiré pattern. Significant variation in the peak position occurs between different moiré cells, likely arising from a randomly varying potential arising from point defects in the material. At the higher temperature of 80 K, we find that the sharp peaks associated with the localized states disappear, although the energy shifts between spectra obtained at corrugation minima and maxima remain.

Figure 1 shows STM images of the MoS_2−WSe_2 heterobilayer, showing its moiré pattern with maxima in the corrugation and two types of minima. We label the spatial locations corresponding to corrugation maxima as A, the minima that are deepest for sample bias of −1.5 V but intermediate in depth for +1.5 V as B, and the other type of minima as C (see Figures 1b−d). The appearance of the moiré corrugation is completely consistent with the prior work of Zhang et al.[7] Those workers demonstrated on the basis of annular dark-field scanning transmission electron microscopy that their CVD-grown material had the MoS_2 and WSe_2 layers stacked with 0° rotational misalignment (as opposed to 180° or some other angle).[7] For our samples, we find the majority of the sample to have a rotational misalignment of either 0° (R-stacking) or 180° (H-stacking), as described in Figure S1. The 0° and 180° cases cannot be distinguished on the basis of STM images alone,[7] and hence, we tentatively utilize the 0° angle determined by Zhang et al. We observe a moiré period of 8.5 ± 0.2 nm, which is consistent with lattice constants of 0.316 and 0.328 nm for MoS_2 and WSe_2, respectively, so that 27 unit cells of MoS_2 fit onto 26 unit cells of WSe_2. Comparing both the STS data presented below and voltage-dependent images shown in Figure S2 to the data of Zhang et al.,[7] the locations that we label A, B, and C are found to correspond, in their notation, to AA, AB_W, and AB_{Se}, respectively. At the A = AA locations, the Mo atoms are directly over the W and the S atoms are directly over the Se; at the B = AB_W locations, the Mo atoms are over the Se atoms and the W atoms are visible through the MoS_2; at the C = AB_{Se} locations, the S atoms are over the W atoms and the Se atoms are visible through the MoS_2 (as shown in Figure 1e and with a full view of moiré unit cell shown in Figure S3). First-principles computations reveal a 0.06 nm difference in the equilibrium separation of MoS_2 and WSe_2 for these various registries, as listed in Table 1 (and in agreement with Zhang et al.).[7] Associated with the differing registries, the theoretical energies of band edges are found to change, as also shown in Table 1 (computed using the Vienna Ab-Initio Simulation Package[27] with the projector-augmented wave method,[28] employing the Purdew−Burke−Ernzerhof generalized gradient approximation exchange-correlation functional[29] together with dipole corrections obtained by Grimme's DFT-D2 method,[30] as further detailed in the Supporting Information). Notation for the labeling of bands is similar to that employed by Zhang et al., according to the point in **k**-space that the band is centered on (Γ, K, or Q) and the layer (W for WSe_2 or M for MoS_2) from which the band originates.[5,7]

Table 1. First-Principles Computational Results for Various Registries (A, B, C) of 1 × 1 unit cell of MoS_2 on WSe_2, Listing the Equilibrium MoS_2−WSe_2 Separation and the Energies of the Γ_W VB and the K_M CB Edges Relative to the Vacuum Level on the WSe_2 Side of the MoS_2−WSe_2 Bilayer

		E (eV) − $E_{VAC,W}$	
registry	separation (nm)	Γ_W	K_M
A = AA	0.690	−5.29	−4.57
B = AB_W	0.632	−5.09	−4.55
C = AB_{Se}	0.629	−5.04	−4.46

Figure 2b shows typical spectra obtained from the MoS_2−WSe_2 heterobilayer, which can be compared with spectra obtained from individual, isolated layers of MoS_2 on epitaxial graphene (EG) and WSe_2 on EG as shown in Figure S4. The

DOI: 10.1021/acs.nanolett.7b05125
Nano Lett. 2018, 18, 1849−1855

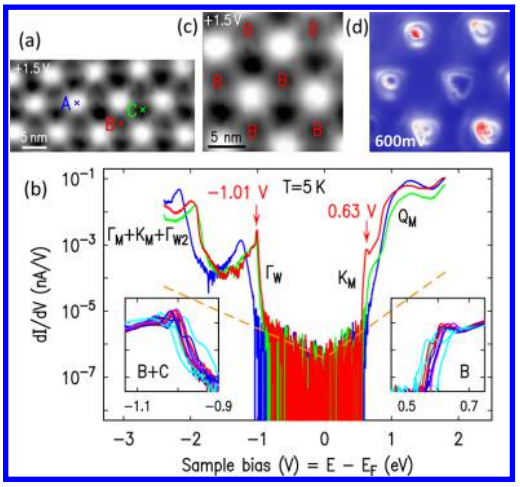

Figure 2. STM and STS data acquired at 5 K showing (a) constant-current image of heterobilayer of MoS_2 on WSe_2, (b) selected spectra acquired at the points indicated in panel a, with insets showing expanded view of band-edge peaks and including data from nearby spatial locations, (c) a constant-current image of heterobilayer, and (d) a constant-height conductance map acquired at 600 mV (same color range as in Figure 3b).

highest lying valence band (VB) of the heterobilayer is labeled Γ_W; this band derives primarily from the WSe_2. It is important to note that a higher VB also exists, centered at the K point and also associated with WSe_2 (K_W band). We can observe that band in spectra of an isolated WSe_2 layer on EG and also for signal-averaged spectra of the heterobilayer (Figure S4), but it is not visible (due to low intensity) in Figure 2 because it originates both from an edge point of the Brillouin zone[31,32] and from the WSe_2 layer that is beneath the MoS_2. The lowest-lying conduction band (CB) in Figure 2a is labeled K_M, deriving primarily from a MoS_2 band centered at the K point of the BZ. Significant differences are seen in the spectra of Figure 2b depending on the location within the moiré unit cell that they are acquired at. For spectra acquired from the A locations (corrugation maxima), we find results similar to those previously presented by Zhang et al.[7] However, if we look to other locations in the unit cell, we obtain significantly different results. Specifically, examining spectra from locations B and C in Figure 2b, we find intense, sharp peaks observed at energies near the band edges of the Γ_W VB and K_M CB. This type of sharp spectral feature from a TMD heterobilayer has not been previously reported.

Expanded views of the sharp band-edge peaks are provided in the insets of Figure 2b, showing spectra obtained from B and C locations (negative bias) or from B locations only (positive bias); additional band-edge spectra are displayed in Figure S5. At the B locations, we find sharp peaks at both the Γ_W VB and K_M CB edges, whereas at the C locations, we only find sharp peaks at the Γ_W VB edge. We use a modulation voltage of V_{mod} = 10 mV rms in the measurements. The corresponding energy resolution[33] (full-width at half-maximum, fwhm) is given by $\Delta E = \sqrt{(3.5kT)^2 + (2.5eV_{mod})^2} = 25.0$ meV at T = 5 K. Many of the Γ_W VB peaks (left inset) are seen to have width very close to this value. Hence, these peaks have intrinsic width considerably less than 10 mV, with the modulation producing the observed width. The dominant peak for these Γ_W VB features lies typically at −1.01 V, with a spread of 10−20 mV in the position of this peak, comparing spectra from different moiré cells. (Our measurement reproducibility for peak positions measured repeatedly at the same location is <1 mV). In contrast, for the K_M CB peaks (right inset), the width of some of these might be limited by the 10 mV modulation, but others appear to be broader. Additionally, there are multiple band-edge peaks in many of those spectra. Nevertheless, closely studying these spectra, we again can see cell-to-cell variation of 10−20 mV in the position of specific peaks in the spectra. We

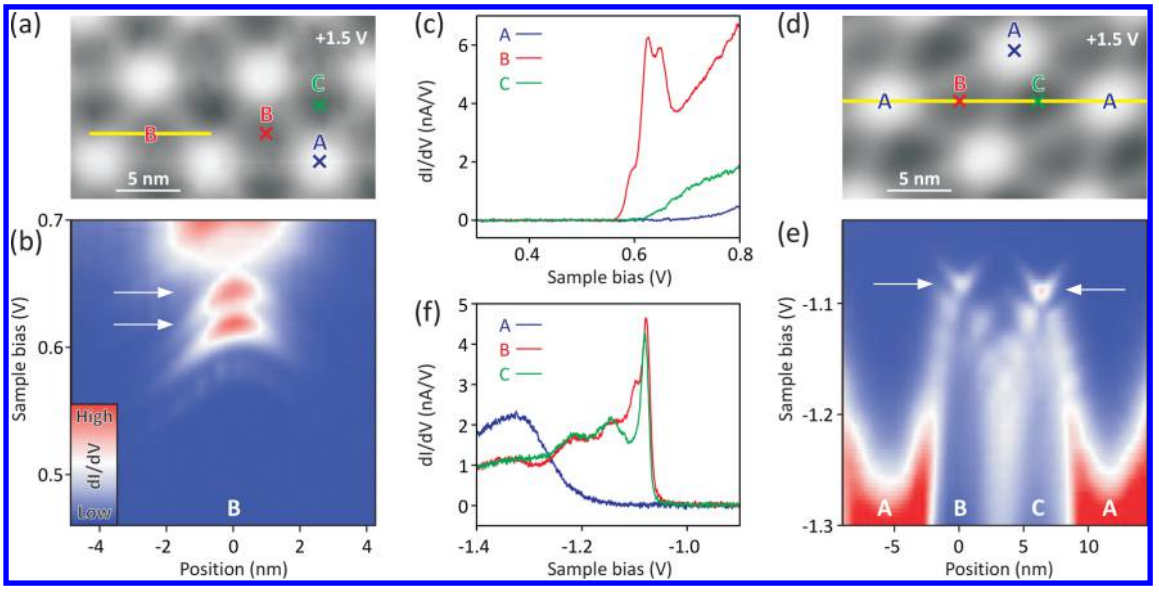

Figure 3. (a) STM image, with moiré locations A, B, and C indicated. (b) Constant-height conductance map taken along the yellow line in panel a for voltages in the conduction band-edge region, revealing two B-confined states (marked by arrows) and the band onset at higher energy (broader B-centered conductance feature). (c) Tunneling spectra recorded as indicated by crosses in panel a. (d) Same as panel a but at a different area of the MoS_2−WSe_2 moiré structure. (e) Constant-height conductance map taken along the yellow line in panel d for voltages in the valence band-edge region; confined states occur at locations B and C. (f) Tunneling spectra recorded as indicated by crosses in panel d. The spectra in panels c and f are recorded with the variable-z method but are not normalized to constant z.

DOI: 10.1021/acs.nanolett.7b05125
Nano Lett. 2018, 18, 1849−1855

attribute the variation in peak position for both the Γ_W and K_M peaks to the influence of a randomly varying potential in the layers, likely due to the point defects in the material (as seen, e.g., in Figure 1c and discussed in ref 25; some defects exhibit midgap states and others do not, but all spectra presented in the present work are acquired sufficiently far from any defect such that no defect states appear in the results). With the width of the spectral peaks being less than their cell-to-cell variation in position, we speculate that it is quite possible that the corresponding states are spatially localized within individual moiré cells (transport through the states would likely still be enabled by their connection to the graphene below the heterobilayer).

Associated with these sharp features we observe electronic states that are spatially confined within the moiré unit cells, an example of which is shown in Figures 2c,d. Figure 2c shows a constant-current topography image with the B locations marked, and Figure 2d shows a constant-height conductance map of the same surface area, acquired at +0.6 V. Distinct rings are seen, confined in the area of the type-B corrugation minima; we associate these features (and the sharp band-edge peaks) with quantum-confined states in the moiré unit cell. At higher voltages, these rings evolve into more extended features within the moiré pattern, associated with extended band states, similar to those presented by Zhang et al.[7] Figure S6 presents additional conductance maps over a wide range of bias voltages.

Additional information on the spatial arrangement of the quantum-confined states near the band edges is obtained by conductance mapping as a function of both energy and spatial position, as shown in Figure 3 for both the Γ_W VB and K_M CB band-edge states. Starting our discussion with the CB states, the conductance was probed with the tip held at constant height and at a given bias along a line spanning a location B as indicated by the yellow line in Figure 3a. Performing this measurement as a function of sample bias yields the spatial conductance map in Figure 3b. A pair of B-confined states are found that are separated by ~30 meV. The V-shaped streaks branching off from the conductance maxima are likely due to tip-induced band bending (TIBB) pushing up the confined-state energy when the tip approaches the location B. The TIBB effect explains also the ring features shown in Figure 2d and their evolution with bias voltage (Figure S6). The spectra in Figure 3c are consistent with the conductance map and reveal a double peak plus a shoulder when the tip probes location B, whereas no confined states occur at locations A and C.

Now turning to the VB states, the conductance map in Figure 3e was taken along a line spanning a location sequence A−B−C−A (as indicated in Figure 3d) at energies around the VB band edge. In this case, confined states are observed at locations B and C (along with the aforementioned TIBB-induced streaks), and again, no confinement occurs at location A. However, the minimum in VB band-edge position at location A (cf. Zhang et al.[7] and Table 1) is clearly visible. Note that the conductance associated with the VB fades out at locations B and C because of the height modulation in the moiré pattern (Figure 1d and Table 1) and the fact that the mapping in Figure 3e was performed at constant tip height. The spectra in Figure 3f complement the measurement in the VB-band edge region and are in agreement with the conductance map in Figure 3e.

Before turning to an explanation for our observed band-edge spectral peaks, we first consider the fact that such features were not reported by Zhang et al.[7] Their studies were conducted at liquid nitrogen temperature (near 77 K), and so to investigate the possible influence of temperature, we also performed studies at 80 K. The results are pictured in Figure 4. We again

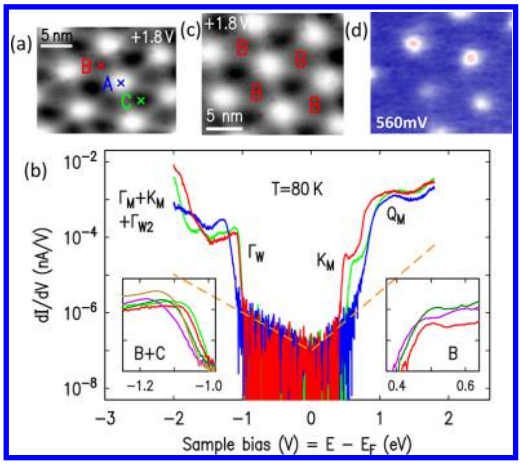

Figure 4. STM and STS data acquired at 80 K, showing (a) a constant-current image of heterobilayer of MoS_2 on WSe_2; (b) tunneling spectra acquired at the locations indicated in panel a, with insets showing expanded view of band-edge peaks and including data from nearby spatial locations; (c) a constant-current image of heterobilayer; and (d) a constant-height conductance map acquired at 560 mV (same color range as in Figure 3b).

observe the moiré pattern over the surface, Figure 4a, and STS measurements at various locations throughout the moiré unit cell reveal shifts in the energies of band edges (Figure 4b), i.e., similar to those seen both by Zhang et al. and in our 5 K measurements. Expanded views of the band edges are shown in the insets of Figure 4b (also including a few additional spectra from nearby locations). Examining the edge of the Γ_W VB (left inset), we find no trace of the sharp spectral features that were found in the 5 K data (Figure 2b, left inset). For the K_M CB, some "sharpening" of the band edge (a slight peak) is still apparent in the 80 K spectra (Figure 4b, right inset), but we do not consider this modest effect to be inconsistent with the prior work.[7] A comparison to the 5 K spectra of Figure 2b reveals that significant broadening of the band-edge features has also occurred for these K_M band-edge states. It should be noted that the 80 K temperature corresponds to kT = 6.9 meV, yielding an energy resolution[33] of $\Delta E = \sqrt{(3.5kT)^2 + (2.5eV_{mod})^2} = 35$ meV, which is only moderately larger than the 25 meV resolution for the 5 K data. Hence, the additional broadening apparent in the 80 K data appears to be considerably larger than expected from either instrumental effects or thermal occupation of electronic states. As a possible mechanism for this broadening, we note that low-energy phonon modes associated with TMD multilayers[34] might, through deformation-potential coupling, act to inhibit the formation of the sharp band-edge states; additional temperature-dependent work is needed to further elucidate this effect. In any case, consistent with these changes in the STS, Figure 4d shows constant-height conductance mapping of the CB edge at 80 K (additional data is provided in Figure S7). Spatial confinement of the states in the moiré unit cell is clearly evident, but in contrast to the 5 K results of Figure 2d, we now find no distinct features that we can associate with discrete quantum states.

Let us now consider the origin of the sharp band-edge spectral peaks seen in the 5 K data. We apply similar reasoning

DOI: 10.1021/acs.nanolett.7b05125
Nano Lett. 2018, 18, 1849−1855

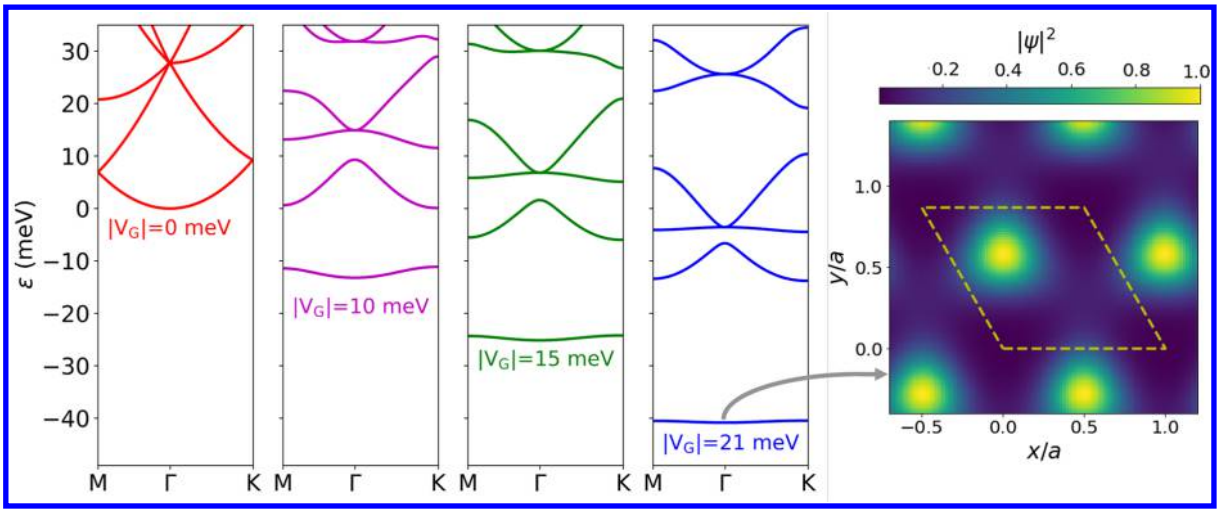

Figure 5. Left: band structures for an NFE model on a hexagonal moiré lattice, employing different magnitudes for the V_G potential terms of the six lowest (nonzero) **G** vectors, $|V_G|$. Right: wave function for the state of the lowest band, at the Γ point, for $|V_G| = 21$ meV.

as used for describing STS spectra arising from the moiré pattern of graphene on hexagonal boron nitride (h-BN),[35,36] although with one very important difference being that, for the MoS_2−WSe_2 system, we are dealing with bands with parabolic dispersion. We construct an effective potential for each band edge in the full moiré unit cell using the band-edge energies of the small, 1 × 1 unit cell computations of Table 1 to estimate the effective potential. This spatially varying potential is constructed as a Fourier series using only the Fourier components at the lowest nonzero reciprocal lattice vectors (potential term V_G on each of three equivalent **G** vectors and V_G^* on the inequivalent set of three **G** vectors).[36] With this effective potential, we then solve the Schrodinger equation for the full moiré unit cell; with only six nonzero V_G terms, the problem is identical to that of a nearly free electron (NFE) model on a 2D hexagonal lattice, except that the "perturbing" V_G terms of the NFE model are now relatively large (compared with the "unperturbed" band widths) for the moiré problem. Assuming an effective mass of unity, then for our 8.5 nm moiré period, the dispersion of the lowest band is only 9.3 meV (e.g., out to the edge of the BZ at the K-point), neglecting the spatially varying terms in the potential. Then, including these terms, the well-known gaps of $2|V_G|$ form at the BZ edges, yielding a bandwidth for the lowest band that is less than this 9.3 meV value. As $|V_G|$ increases, the width of the lowest band decreases and it shifts to lower energies, as shown in Figure 5.

Concerning the size of the $|V_G|$ terms,[36] an important contribution, already discussed by Zhang et al. in connection with their observed band shifts,[7] arises from hybridization of the states between MoS_2 and WSe_2. In particular, the Γ_W state derived from the WSe_2 Γ-point VB is significantly perturbed by the adjoining MoS_2, producing a higher-lying state (i.e., nearer to the VB edge) at the corrugation minimum compared to a maximum. Table 1 lists the corresponding energies of this band edge relative to the vacuum level on the WSe_2 side of the bilayer (the EG below the heterobilayer is known to have large n-type doping,[37] so using the electrostatic potential energy below the WSe_2 as a reference is appropriate). Considering the variation of this band-edge energy over the moiré cell, with the method of Jung et al.,[36] we obtain $|V_G^{\Gamma W}| = 21$ meV; the NFE band structure of this case, as shown in Figure 5, has a width of the lowest lying band of only 0.4 meV. We associate this band with the sharp (resolution limited) band-edge VB states seen in Figures 3 and 4. Figure 5 (right) shows the wave function at the Γ-point associated with this lowest band. We find strong confinement of the state within the moiré unit cell, consistent with experiment.

The confined states shown in Figure 5 provide a qualitative explanation for the spectral peaks that we observe near the Γ_W VB edge, except that in experiment these states are observed at both of the B and C corrugation minima (Figure 3b), whereas in our theory described thus far, we expect such states only at the C minima (Table 1, third column, with the VB Γ_W band-edge energy at the C minimum being highest). However, we find nearly the same energies (within 50 meV) for the B and C minima, and we note that the prior theoretical results of Zhang et al.[7] (which include strain corrections) find the energies at the two minima to be equal within 20 meV with the B minima energy being highest.

Turning to the origin of the spectral peaks observed near the K_M CB edge, the energies of the effective potential for this band edge are listed in the final column of Table 1. We see that the potential has nearly equal (within 20 meV) minima at the A and B locations, contrary to experiment in which the states are clearly confined to the B locations. However, we feel that detailed electrostatic modeling of the MoS_2−WSe_2-EG system, including the presence of the STM probe-tip, is necessary to fully understand the potential variation across the moiré unit cell. In particular, intrinsic (polarization) dipoles exist across the MoS_2−WSe_2 bilayer, with substantial variation in dipole energy across the unit cell (0.076, 0.165, and 0.071 eV at the A, B, and C locations, respectively, where in all cases, the electronic energy increases from the WSe_2 to the MoS_2 layer). Bound charge associated with the dipoles will be screened (nonlinearly) by induced free charge in the EG, which will produce further variations in energy across the unit cell. This screening effect of the EG is affected by its electron doping,[37] which will be large for sample bias of ≤ 0 but relatively small for bias of $\gg 0$. Such effects must be modeled in detail before the locations of the quantum-confined states can be fully understood.

In summary, at a temperature of 5 K, we observe single-particle quantum-confined states associated with the Γ_W VB and K_M CB in a MoS_2−WSe_2 heterobilayer. Such states have

DOI: 10.1021/acs.nanolett.7b05125
Nano Lett. 2018, 18, 1849−1855

not been previously experimentally reported in TMD heterobilayers to our knowledge (although their presence is implicit in an early theoretical study[9] as well as in two recent theoretical investigations of multiparticle effects),[38,39] but we believe that they are a general property of such systems. The states in our experiments turn out to be confined at the minima of the moiré corrugation, but this need not be the case for other bilayers (or even for the MoS_2−WSe_2 in the absence of a biased STM probe-tip or an underlying EG layer). The method of analysis we propose is the same as previously employed for graphene on h-BN,[36] with one crucial difference being that it is parabolic bands in the MoS_2 and WSe_2 that are perturbed by the moiré (unlike the highly dispersive, linear bands of graphene), leading to the confined states in the MoS_2−WSe_2 heterobilayer. We observe resolution-limited spectral peaks for the Γ_W band-edge states in particular, with significant variation in those energies between moiré unit cells, suggestive of spatial localization of the states within a single cell. We also observe a rather large temperature dependence for these states, leading to their absence in observations at 80 K. As already suggested by Zhang et al., the large modulation in band edge positions observed for these TMD heterobilayers may be relevant for device application.[7] For example, the sharp, localized band-edge states observed here (at 5 K), in analogy with localized states of coupled quantum dots, might serve as a useful platform for quantum computation.[40] However, the band-edge shifts observed both at 5 K and higher temperatures may be detrimental for application of such heterobilayers in interlayer tunneling devices.[41] Additional work is required to more fully determine the impact of the band-edge shifts and concomitant band-edge states in device applications.

■ ASSOCIATED CONTENT

Supporting Information

The Supporting Information is available free of charge on the ACS Publications website at DOI: 10.1021/acs.nanolett.7b05125.

Additional experimental details. Figures showing STM topography, bias-dependent constant-current STM images, a ball-and-stick structure model, STS, detailed scanning tunneling spectra, and constant-height conductance maps. (PDF)

■ AUTHOR INFORMATION

Corresponding Author

*E-mail: feenstra@cmu.edu.

ORCID

Yu-Chuan Lin: 0000-0003-4958-5073
Joshua A. Robinson: 0000-0001-5427-5788
Randall M. Feenstra: 0000-0001-7120-5685

Author Contributions

Y.P., S.F, and R.M.F. carried out the STM experiments, and they wrote the paper with inputs from other authors. Y.N. performed the first-principles computations under the supervision of K.C. D.W. performed the NFE modeling. Y.C.L., B.J., and K.Z. grew the samples, under the supervision of J.A.R.

Notes

The authors declare no competing financial interest.

■ ACKNOWLEDGMENTS

We gratefully acknowledge discussions with D. Xiao, M. Widom, and V. Bheemarasetty (all of CMU), M. Hybertsen (Brookhaven), and V. Meunier (Rennselaer). This work was supported in part by the A. von Humboldt Foundation and by the Center for Low-Energy Systems Technology (LEAST), one of six centers of STARnet, a Semiconductor Research Corporation program sponsored by Microelectronics Advanced Research Corporation (MARCO) and Defense Advanced Research Projects Agency (DARPA).

■ REFERENCES

(1) Geim, A. K.; Grigorieva, I. V. *Nature* **2013**, *499*, 419−425.
(2) Mak, K. F.; Lee, C.; Hone, J.; Shan, J.; Heinz, T. F. *Phys. Rev. Lett.* **2010**, *105*, 136805.
(3) Wang, Q. H.; Kalantar-Zadeh, K.; Kis, A.; Coleman, J. N.; Strano, M. S. *Nat. Nanotechnol.* **2012**, *7*, 699−712.
(4) Li, M.-Y.; Shi, Y.; Cheng, C. C.; Lu, L.-S.; Lin, Y.-C.; Tang, H.-L.; Tsai, M.-L.; Chu, C.-W.; Wei, K.-H.; He, J.-H.; Chang, W.-H.; Suenaga, K.; Li, L.-J. *Science* **2015**, *349*, 524−528.
(5) Yun, W. S.; Han, S. W.; Hong, S. C.; Kim, I. G.; Lee, J. D. *Phys. Rev. B: Condens. Matter Mater. Phys.* **2012**, *85*, 033305.
(6) Chiu, M.-H.; Li, M.-Y.; Zhang, W.; Hsu, W.-T.; Chang, W.-H.; Terrones, M.; Terrones, H.; Li, L.-J. *ACS Nano* **2014**, *8*, 9649−9656.
(7) Zhang, C.; Chuu, C.-P.; Ren, X.; Li, M.-Y.; Li, L.-J.; Jin, C.; Chou, M.-Y.; Shih, C.-K. *Sci. Adv.* **2017**, *3*, e1601459.
(8) Lin, Y. C.; Ghosh, R. K.; Addou, R.; Lu, N.; Eichfeld, S. M.; Zhu, H.; Li, M.-Y.; Peng, X.; Kim, M. J.; Li, L.-J.; Wallace, R. M.; Datta, S.; Robinson, J. A. *Nat. Commun.* **2015**, *6*, 7311.
(9) Kang, J.; Li, J.; Li, S.-S.; Xia, J.-B.; Wang, L.-W. *Nano Lett.* **2013**, *13*, 5485−5490.
(10) Tongay, S.; Fan, W.; Kang, J.; Park, J.; Koldemir, U.; Suh, J.; Narang, D. S.; Liu, K.; Ji, J.; Li, J.; Sinclair, R.; Wu, J. *Nano Lett.* **2014**, *14*, 3185−3190.
(11) Kang, J.; Tongay, S.; Zhou, J.; Li, J.; Wu, J. *Appl. Phys. Lett.* **2013**, *102*, 012111.
(12) Chiu, M.-H.; Zhang, C.; Shiu, H.-W.; Chuu, C.-P.; Chen, C.-H.; Chang, C.-Y. S.; Chen, C.-H.; Chou, M.-Y.; Shih, C.-K.; Li, L.-J. *Nat. Commun.* **2015**, *6*, 7666.
(13) Rivera, P.; Seyler, K. L.; Yu, H.; Schaibley, J. R.; Yan, J.; Mandrus, D. G.; Yao, W.; Xu, X. *Science* **2016**, *351*, 688−691.
(14) Rivera, P.; Schaibley, J. R.; Jones, A. M.; Ross, J. S.; Wu, S.; Aivazian, G.; Klement, P.; Seyler, K.; Clark, G.; Ghimire, N. J.; Yan, J.; Mandrus, D. G.; Yao, W.; Xu, X. *Nat. Commun.* **2015**, *6*, 6242.
(15) Hong, X.; Kim, J.; Shi, S.-F.; Zhang, Y.; Jin, C.; Sun, Y.; Tongay, S.; Wu, J.; Zhang, Y.; Wang, F. *Nat. Nanotechnol.* **2014**, *9*, 682−686.
(16) Hermann, K. *J. Phys.: Condens. Matter* **2012**, *24*, 314210.
(17) Hunt, B.; Sanchez-Yamagishi, J. D.; Young, A. F.; Yankowitz, M.; LeRoy, B. J.; Watanabe, K.; Taniguchi, T.; Moon, P.; Koshino, M.; Jarillo-Herrero, P.; Ashoori, R. C. *Science* **2013**, *340*, 1427−1430.
(18) Kumar, H.; Er, D.; Dong, L.; Li, J.; Shenoy, V. B. *Sci. Rep.* **2015**, *5*, 10872.
(19) Dean, C. R.; Wang, L.; Maher, P.; Forsythe, C.; Ghahari, F.; Gao, Y.; Katoch, J.; Ishigami, M.; Moon, P.; Koshino, M.; Taniguchi, T.; Watanabe, K.; Shepard, K. L.; Hone, J.; Kim, P. *Nature* **2013**, *497*, 598−602.
(20) Xue, J.; Sanchez-Yamagishi, J.; Bulmash, D.; Jacquod, P.; Deshpande, A.; Watanabe, K.; Taniguchi, T.; Jarillo-Herrero, P.; LeRoy, B. J. *Nat. Mater.* **2011**, *10*, 282−285.
(21) Kim, H. S.; Gye, G.; Lee, S.-H.; Wang, L.; Cheong, S.-W.; Yeom, H. W. *Sci. Rep.* **2017**, *7*, 12735.
(22) Wu, F.; Lovorn, T.; MacDonald, A. H. *Phys. Rev. Lett.* **2017**, *118*, 147401.
(23) Eichfeld, S. M.; Colon, V. O.; Nie, Y.; Cho, K.; Robinson, J. A. *2D Mater.* **2016**, *3*, 25015.

DOI: 10.1021/acs.nanolett.7b05125
Nano Lett. 2018, 18, 1849−1855

(24) Subramanian, S.; Deng, D. D.; Xu, K.; Simonson, N.; Wang, K.; Zhang, K. H.; Li, J.; Feenstra, R.; Fullerton-Shirey, S. K.; Robinson, J. A. *Carbon* **2017**, *125*, 551.
(25) Lin, Y.-C.; Jariwala, B.; Bersch, B. M.; Xu, K.; Nie, Y.; Wang, B.; Eichfeld, S. M.; Zhang, X.; Choudhury, T. H.; Pan, Y.; Addou, R.; Smyth, C. M.; Li, J.; Zhang, K.; Haque, M. A.; Fölsch, S.; Feenstra, R. M.; Wallace, R. M.; Cho, K.; Fullerton-Shirey, S. K.; Redwing, J. M.; Robinson, J. A. *ACS Nano* 2018, 10.1021/acsnano.7b07059.
(26) Mårtensson, P.; Feenstra, R. M. *Phys. Rev. B: Condens. Matter Mater. Phys.* **1989**, *39*, 7744.
(27) Kresse, G.; Furthmüller, J. *Phys. Rev. B: Condens. Matter Mater. Phys.* **1996**, *54*, 11169.
(28) Kresse, G.; Joubert, D. *Phys. Rev. B: Condens. Matter Mater. Phys.* **1999**, *59*, 1758.
(29) Perdew, J. P.; Burke, K.; Ernzerhof, M. *Phys. Rev. Lett.* **1996**, *77*, 3865; erratum. *Phys. Rev. Lett.* **1997**, *78*, 1396.
(30) Grimme, S. *J. Comput. Chem.* **2006**, *27*, 1787.
(31) Stroscio, J. A.; Feenstra, R. M.; Fein, A. P. *Phys. Rev. Lett.* **1986**, *57*, 2579.
(32) Hill, H. M.; Rigosi, A. F.; Rim, K. T.; Flynn, G. W.; Heinz, T. F. *Nano Lett.* **2016**, *16*, 4831−4837.
(33) Morgenstern, M. *Surf. Rev. Lett.* **2003**, *10*, 933.
(34) Zhao, Y.; Luo, X.; Li, H.; Zhang, J.; Araujo, P. T.; Gan, C. K.; Wu, J.; Zhang, H.; Quek, S. Y.; Dresselhaus, M. S.; Xiong, Q. *Nano Lett.* **2013**, *13*, 1007−1015.
(35) Yankowitz, M.; Xue, J.; Cormode, D.; Sanchez-Yamagishi, J. D.; Watanabe, K.; Taniguchi, T.; Jarillo-Herrero, P.; Jacquod, P.; LeRoy, B. J. *Nat. Phys.* **2012**, *8*, 382−386.
(36) Jung, J.; DaSilva, A. M.; MacDonald, A. H.; Adam, S. *Nat. Commun.* **2015**, *6*, 6308.
(37) Ristein, J.; Mammadov, S.; Seyller, Th. *Phys. Rev. Lett.* **2012**, *108*, 246104.
(38) Yu, H.; Liu, G.-B.; Tang, J.; Xu, X.; Yao, W. *Sci. Adv.* **2017**, *3*, e1701696.
(39) Wu, F.; Lovorn, T.; MacDonald, A. H. *Phys. Rev. Lett.* **2017**, *118*, 147401.
(40) Eriksson, M.; Coppersmith, S. N.; Lagally, M. G. *MRS Bull.* **2013**, *38*, 794−801.
(41) Li, J.; Nie, Y.; Cho, K.; Feenstra, R. M. *J. Electron. Mater.* **2017**, *46*, 1378.

DOI: 10.1021/acs.nanolett.7b05125
Nano Lett. 2018, 18, 1849−1855